Chapter 04: Processing and Characterization of Aluminium Matrix Composite

4.1   Preamble

As reported earlier, as-cast composites were found to have few casting defects such as voids, agglomeration/clusters of Silicon Carbide (SiC) particles and particle free regions. Thus, it becomes necessary to perform post processing treatment for further enhancement of metallurgical, mechanical and tribological characteristics of as-cast composites. The present study makes use of a solid state processing technique known as Friction Stir Processing (FSP) to alter the metallurgical, mechanical and tribological properties of as-cast composites. Subsequent topics will discuss the methodology adopted for the performance of FSP on as-cast composites and the characterization of processed composites.

4.2   Outline of Experiments

The critical parameters for FSP are rotational speed, transverse speed, tool tilt angle and tool design. In the present investigation, a commonly adopted tool design was considered and the feasibility trials were conducted by varying tool rotational speed, transverse speed and tilt angle. Depending upon the feasibility trials, process parameters were selected for final experiments and processing of as-cast composites was attempted. Subsequently, microstructural, mechanical and tribological characteristics of the processed composites were studied and compared with that of as-cast composites.

4.3   Experimental Setup, Tooling and Fixture

The present section focuses on details of the experimental setup using which FSP was performed. Furthermore, the section provides details of the FSP tool and fixture using which as-cast composites were firmly hold.

4.3.1 FSP Machine and Fixture

As shown in Figure 4.1, 3-axis automatic vertical milling machine was used for the performance of FSP. Along with the vertical milling machine, Figure 4.1 also represents

the range of spindle rotational speed and transverse speed which is 35-1500 rpm and 20-800 mm/min respectively. The vertical milling machine has an allowance for tilting the spindle by ±50°. It should be noted that the FSP tool generates huge axial and transverse load during the processing due to which plastic deformation and heat generation occurs. Owing to this, the workpiece may experience thermal expansion along with distortion and buckling. Hence, a stiff fixture with higher heat resistance capacity was employed for the performance of FSP.

Figure 4.1 3-Axis automatic vertical milling machine used for FSP

The schematic diagram of the fixture used for performing FSP is shown in Figure 4.2. The fixture was designed such that it constrains the lateral movement of the workpiece under the action of the axial load from the FSP tool. Furthermore, clamping of the workpiece was obtained by 2 straps having 4 M10 size bolts which restrict the vertical movement of workpiece material. A mild steel plate was used as a backing material which not only supports the workpiece material but also protects the fixture cavity from any undulation caused due to the FSP tool. The fixture consisting of workpiece material with backing plate and mounted on vertical milling machine bed is shown in Figure 4.3.
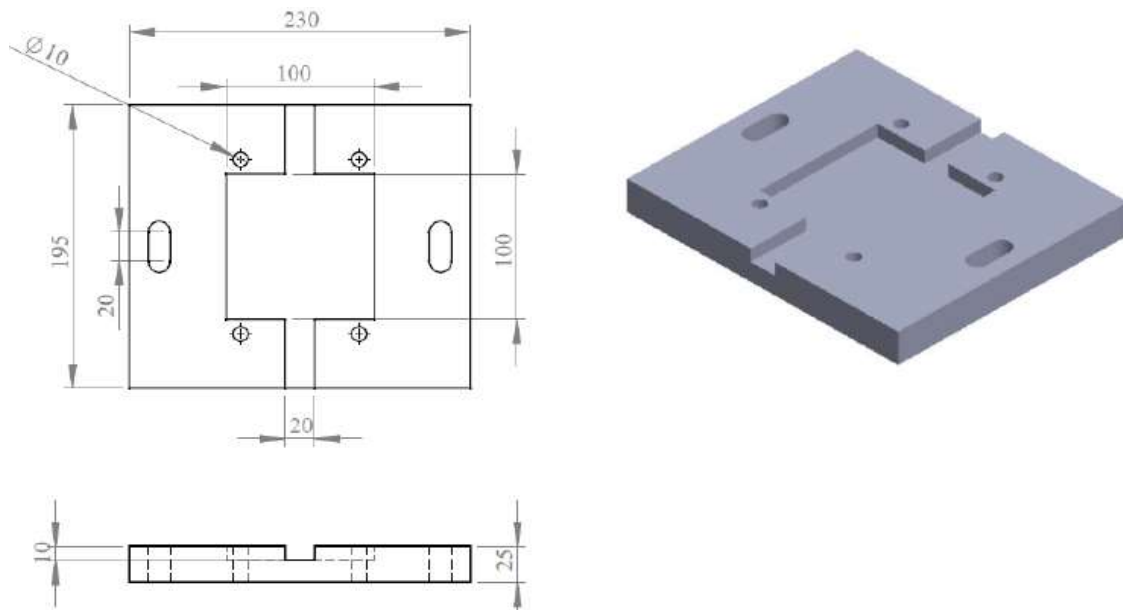
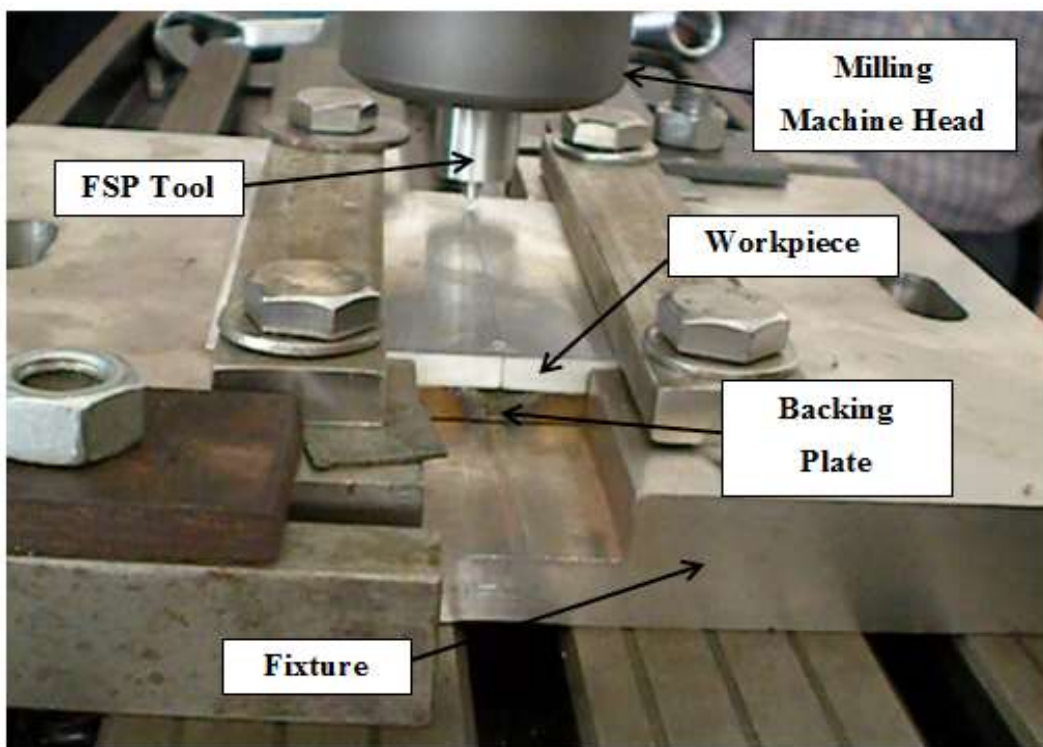Figure 4.2 Schematic representation of fixture

Figure 4.3 Fixture holding a workpiece on vertical milling machine bed

4.3.2 Tool Design

In the present investigation, FSP was implemented for the processing of as-cast composites and not for the manufacturing of surface composites. Due to the same, clapping pass was avoided and only stirring pass was performed. A taper cylindrical

threaded pin was considered for the present investigation. The tool was having a shoulder diameter of 19 mm, pin length of 5.7 mm, the larger diameter of the pin was 6 mm and the smaller diameter of the pin was 3 mm. The stirring tool was fabricated from an H13 rod as per the design represented in Figure 4.4. Post fabrication, the tool was heat treatment for enhancing the hardness of the tool and the final fabricated tool is represented in Figure 4.5.
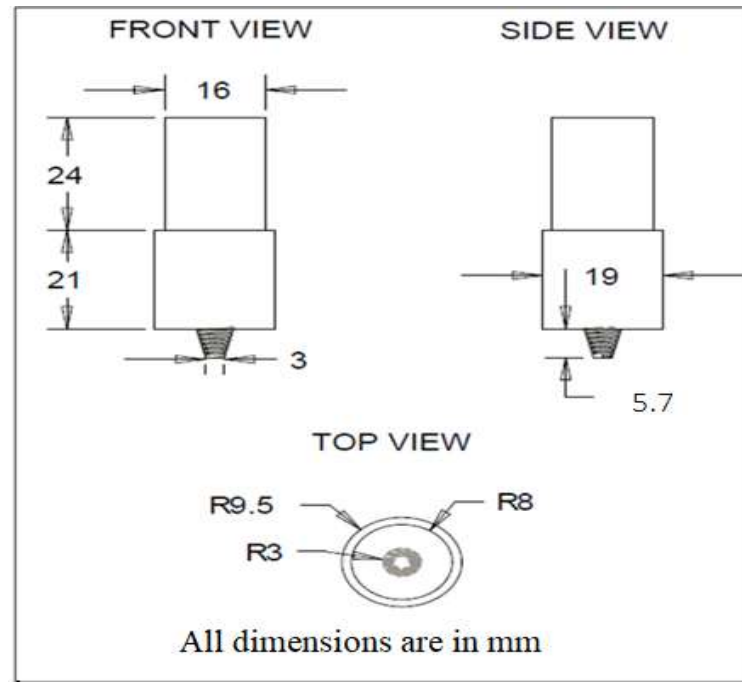

Figure 4.4 Dimensions of taper cylindrical threaded tool

Figure 4.5 Fabricated tool for FSP

4.4   Performance of Experiments

In the present study, clapping pass of FSP was avoided and directly the stirring pass as only processing of as-cast composites was intended. Totally 10 trial experiments were performed to understand the behaviour of the material under different process parameters. The considered process parameters were rotational speed (1500 rpm – 190 rpm), transverse speed (31.5 mm/min – 78 mm/min) and tool tilt angle (0° and 2°). The surface morphology of composites processed with different combinations of process parameters and the trial names is shown in Table 4.1. While comparing trial T2 and T3, it can be observed that an increase in tool tilt angle from 0° to 2° tends to improve the bead width of the weld as well as reduces the defects. Thus for the rest of the trial experiments, the constant tilt angle of 2° was considered. Out of the 10 trial experiments, trial numbers T7 and T9 showed promising results as the processed surface showed the presence of no/minimum visual defects. Thus, trial numbers T7 and T9 were considered for the processing of as-cast composites. For characterization, the specimens required for respective testing were taken from the processed zone as per the schematic shown in Figure 4.6. Microstructural characterization of processed composites was done using Optical Microscopy (OM). The sample preparation for observing microstructure remains the same as discussed earlier. Apart from this, microhardness and wear tests were also performed on processed composites. At last, the evaluated characteristics of processed composites were compared with the respective characteristics of as-cast composites.

Table 4.1 Process parameter of trial experiments and surface morphology of the processed composite (cont.)

Trial No.	Rotational Speed (rpm)	Transverse Speed (mm/min)	Tilt Angle	Surface Morphology
T1	1500	31.5	2°	

Table 4.1 Process parameter of trial experiments and surface morphology of the processed composite (cont.)

Trial No.	Rotational Speed (rpm)	Transverse Speed (mm/min)	Tilt Angle	Surface Morphology
T2	380	78	0°	
T3	380	78	2°	
T4	545	78	2°	
T5	545	50	2°	
T6	765	78	2°	
T7	270	78	2°	

Table 4.1 Process parameter of trial experiments and surface morphology of the processed composite (cont.)

Trial No.	Rotational Speed (rpm)	Transverse Speed (mm/min)	Tilt Angle	Surface Morphology
T8	190	78	2°	
T9	190	50	2°	
T10	190	31.5	2°	

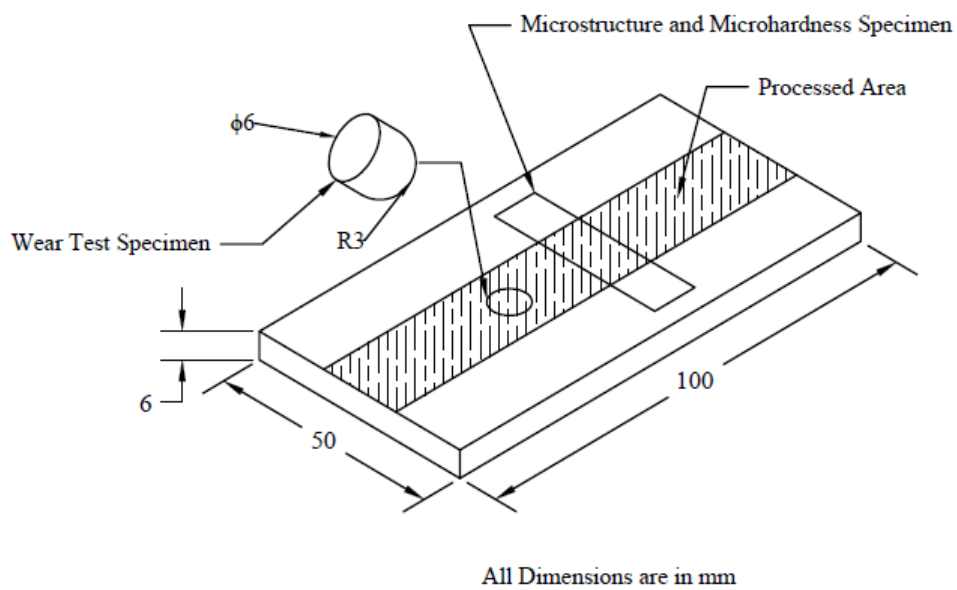Figure 4.6 Schematic representing the specimens taken from the processed zone

4.5 Metallurgical Investigation

The present section discusses the result of the macrostructure and microstructural investigation of the processed composites. Along with this, microhardness results have also been presented. The obtained results are compared with as-cast composites and critical comments have been made.

4.5.1 Macrostructure and Microstructure of Processed Composites

The macrostructure of the processed specimens under two different processing conditions is shown in Figure 4.7. From the existing literature, it has been observed that the macrostructure of processed composites was characterized by four different zones i.e. Nugget Zone (NZ), Thermomechanically Affected Zone (TMAZ), Heat Affect Zone (HAZ) and unprocessed composite (Mondal, Das, Hong, Jeong, & Han, 2019). It should be noted that the macrostructure of all processed composites revealed clear boundaries between NZ and TMAZ on AS. The flow of plasticized material will be higher on AS compared to RS and due to this, the boundary line between NZ and TMAZ is clearly visible on AS. Apart from this, it has been reported that boundaries between NZ and TMAZ were not visible for specimens processed at higher heat input (Ma, 2008). In the present investigation, processing of fabricated composites has been accomplished at a comparatively lower rotational speed. This will result in lower heat generation and owing to this clear boundary between NZ and TMAZ is visible.

It can be observed that NZ of T7 processed composites revealed alternate bands on AS. However, with the increase in weight percent of SiC particles number of alternating bands, the width of bands and spacing between bands were found to reduce. On the other hand, no bands or a comparatively lower number of bands were observed for T9 processed specimens. The characteristic of these bands and the reason behind the formation of bands have been discussed in subsequent sections. Apart from this, T7 processed AA 2014 + 5% SiC and AA 2014 +15% SiC revealed a pinhole near the boundary separating NZ and TMAZ.
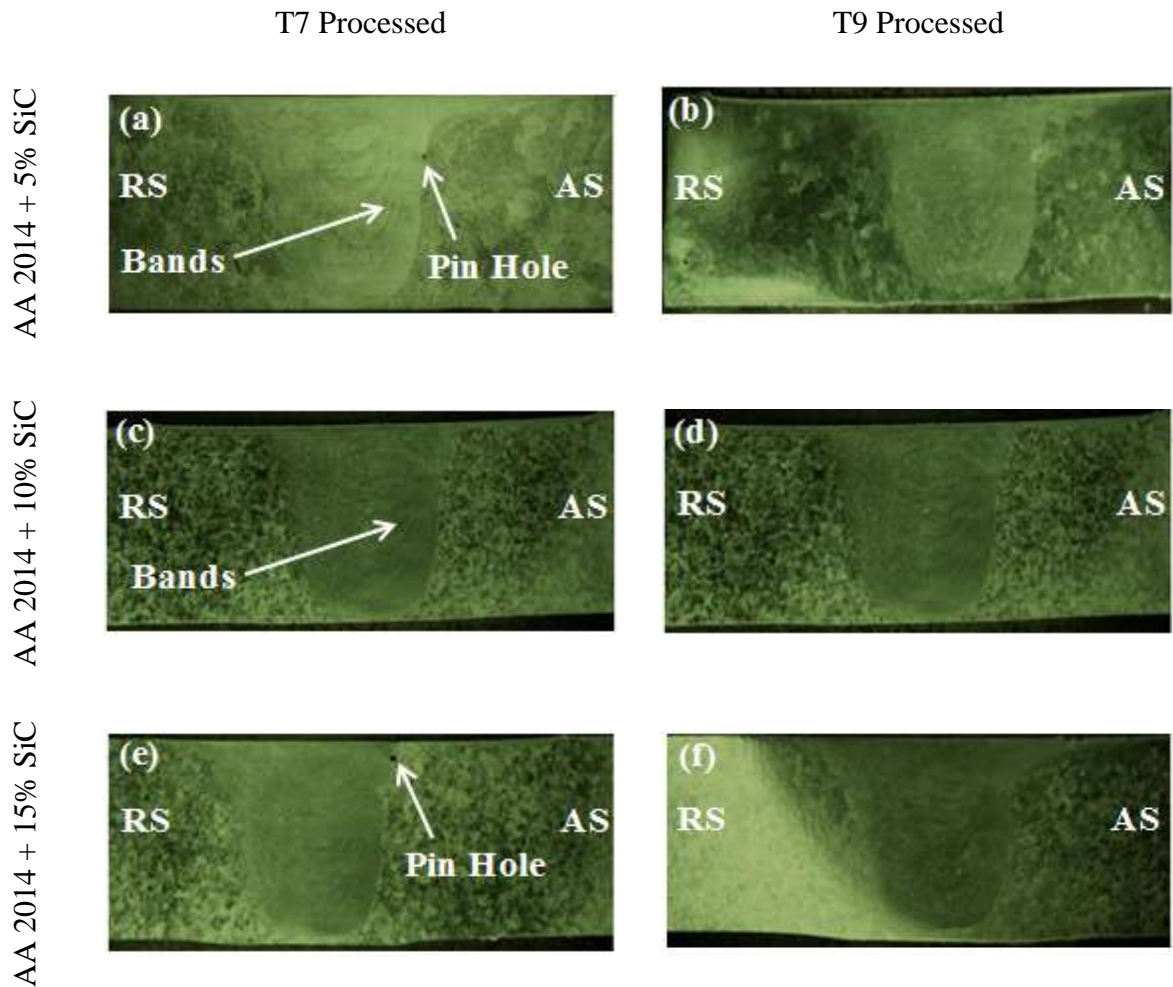
Figure 4.7 Macrostructure of processed composites

Material properties, heat generated during processing, axial force, rotational speed and transverse speed are the dominating parameters that regulate the shape and size of all FSP zones (Bharti, Ghetiya, & Patel, 2020). The friction between the rotating tool and workpiece tends to generate heat which will cause dynamic recrystallization in various zones of FSP. Owing to the stirring action of the rotating tool, extensive plastic deformation will be generated in NZ and TMAZ (Khodabakhshi, Simchi, Kokabi, Gerlich, & Nosko, 2015). Due to this severe plastic deformation and extensive heat generation, NZ will undergo dynamic recrystallization. However, it should be noted that TMAZ will experience the thermal history and comparatively lesser plastic deformation due to which dynamic recrystallization will not occur. On the other side, deformation in HAZ will occur only due to frictional heat and this zone will not undergo plastic deformation. NZ will be characterized by the highest grain refinement whereas; TMAZ will be having an elongated grain structure (Uematsu & Tokaji, 2010).

Micrographic images from NZ of AA 2014 + 5% SiC processed at two different conditions i.e. T7 and T9 are shown in Figure 4.8 (a) and (b). As a result of stirring action created by rotating tool and frictional heat generated during processing, NZ will be subjected to high strain deformation. NZ is the zone that was previously occupied by the tool pin and thus material in NZ will undergo dynamic recrystallization (Bharti, Ghetiya, & Patel, 2020). The material in and around the tool pin will be subjected to extensive plastic deformation along with grain fragmentation. Due to the high strain deformation and dynamic recrystallization, NZ was found to characterize by equiaxed and fine grain structure. Also from Figure 4.8 (a) and (b), it can be observed that NZ of processed composites is characterized by globular grains of smaller dimensions. At the same time, NZ of both the processed composites revealed the presence of finer size of SiC particles. Irrespective of processing conditions, it can be observed that fine SiC particles are homogeneously distributed in NZ. Apart from this, NZ of AA 2014 + 5% SiC processed at T7 condition was found to have banded microstructure. From Figure 4.8(a), it can be observed that NZ exhibit two discernible alternating bands which are randomly labelled as Band A and Band B. In both the bands, the presence of SiC particles can be observed. However, Band A was characterised by fine, round and equiaxed grain structure whereas, Band B was found to have fine, long and elongated grains. Thus, it can be observed that grain sizes in Band A are smaller compared to that of Band B. Previously, Sutton et al., (2002) and Yang et al., (2004) reported similar banded structures in 2xxx series of aluminium. For the 2xxx series of aluminium, these banded structures can be observed with a decrease in welding speed or decrease in maximum weld temperature. It was reported that spacing between the bands was corresponding to tool transverse per revolution (Sutton, Yang, Reynolds, & Taylor, 2002). However, it should be noted that the banded structure in AA 2014 +5% SiC (Figure 4.8(b)) processed by T9 condition were visible but it was difficult to differentiate. Also for the T9 condition, a comparatively lower number of bands was observed.

Similar to AA 2014 + 5% SiC, NZ of other composites i.e. AA 2014 + 10% and 15% SiC processed at both conditions showed a fine, equiaxed and homogenous distribution of SiC particles. The same can be observed from Figure 4.8(c) - (f). It can be observed that NZ of all processed composites is free from several major processing defects such as deficiency/extensive in plastic deformation, deficiency in heat input, porosity, groves and many more. Referring to Figure 4.8(c), the presence of a banded

structure can be observed for AA 2014 + 10% SiC processed by T7 conditions. This banded structure was nearly similar to the banded structure that was earlier reported Figure 4.8(a). However, NZ of AA 2014 + 10% SiC (Figure 4.8(c)) showed a reduction in the width of Band A and Band B. On the other side, NZ of AA 2014 + 10% SiC processed by T9 condition didn't portrait the presence of banded structure. As represented in Figure 4.8(d), NZ of composite processed by T9 condition was found to have the presence of two different zones which are randomly named as Zone A and Zone B. It can be observed that Zone A represented in Figure 4.8(d) is particle rich region. Zone A was found to have a finely distributed round shape of SiC particles. Apart from this, Zone A was found to have few elongated grains of SiC particles and few clusters. Whereas, Zone B can be termed as particle deficient region, where the presence of SiC particles was comparatively less dense. As reported earlier, the presence of banded structure was observed for T9 processed AA 2014 + 5 % SiC but it was difficult to differentiate those bands within NZ. It can be observed that the lesser number of bands which were observed in Figure 4.8(b) were found to disappear and resulting NZ of T9 processed AA 2014 +10% SiC was found to have particles rich and particle deficient zones. This formation of zones and vanishing of bands could be attributed to an increase in the weight percentage of reinforcement particles. Referring to Figure 4.8(e), the banded structure of NZ can be observed. Compared to the other two compositions, a lower number of bands can be observed in AA 2014 + 15% SiC. At the same time, Figure 4.8(e) shows comparatively higher grain refinement than that AA 2014 + 5% SiC and AA 2014 + 10% SiC. Thus, on comparing Figure 4.8 (a), (c) and (e) it can be observed that an increase in weight percent of SiC particles causes a reduction in banded structure as well as a reduction in the width of the band. However, an increase in weight percent of SiC particles leads to grain refinement in both the identified bands. Similarly, comparing Figure 4.8(b), (d) and (f) it can be observed that an increase in weight percent of SiC particles tends to reduce the formation of a banded structure or zone formation in NZ. Figure 4.8(f) reports fine and equiaxed grains of SiC particles which are homogeneously distributed in the entire NZ. NZ of AA 2014 + 15% SiC particles reported that formation of banded structure/particle rich zone/particle deficient zone doesn't take place and SiC particles are uniformly distributed.

FSP tend to create a transition zone or TMAZ between the NZ and parent material (Mishra & Ma, 2005). As discussed earlier, TMAZ will be subjected to both temperature

and deformation but will not undergo dynamic recrystallization. Thus, TMAZ will be characterized by deformed and elongated grain structure. Figure 4.9 represents microstructural images from TMAZ of AA 2014 + 5% SiC processed by both conditions. From Figure 4.9(a) and (b), the presence of elongated/needle shaped grains can be observed. These grains in TMAZ were deformed in an upward flowing pattern around NZ. Owing to the stirring effect generated by the rotating tool, it can be observed that the grains in TMAZ are narrow down and converge towards NZ. Due to the lack of plastic deformation, insufficient deformation can be observed in the microstructure of TMAZ. It should be noted that dynamic recrystallization will not occur but the dissolution of several precipitates might take place in TMAZ. The amount of dissolution depends upon the thermal history experienced by this zone during the FSP process (Behnagh, Givi, & Akbari, 2012). The significant point here is that at higher tool rotational speed, the rotating tool will generate a higher centrifugal force which will drag SiC particles away from the pin area and propel them from NZ to TMAZ. Owing to this reason, densification of SiC particles can be observed in the TMAZ of T7 processed composite. This densification and rarefaction of SiC particles can also occur due to thermally induced volumetric changes. Similar observations were made for the remaining two composites, in which TMAZ of T7 processed composites were having densification of SiC particles.
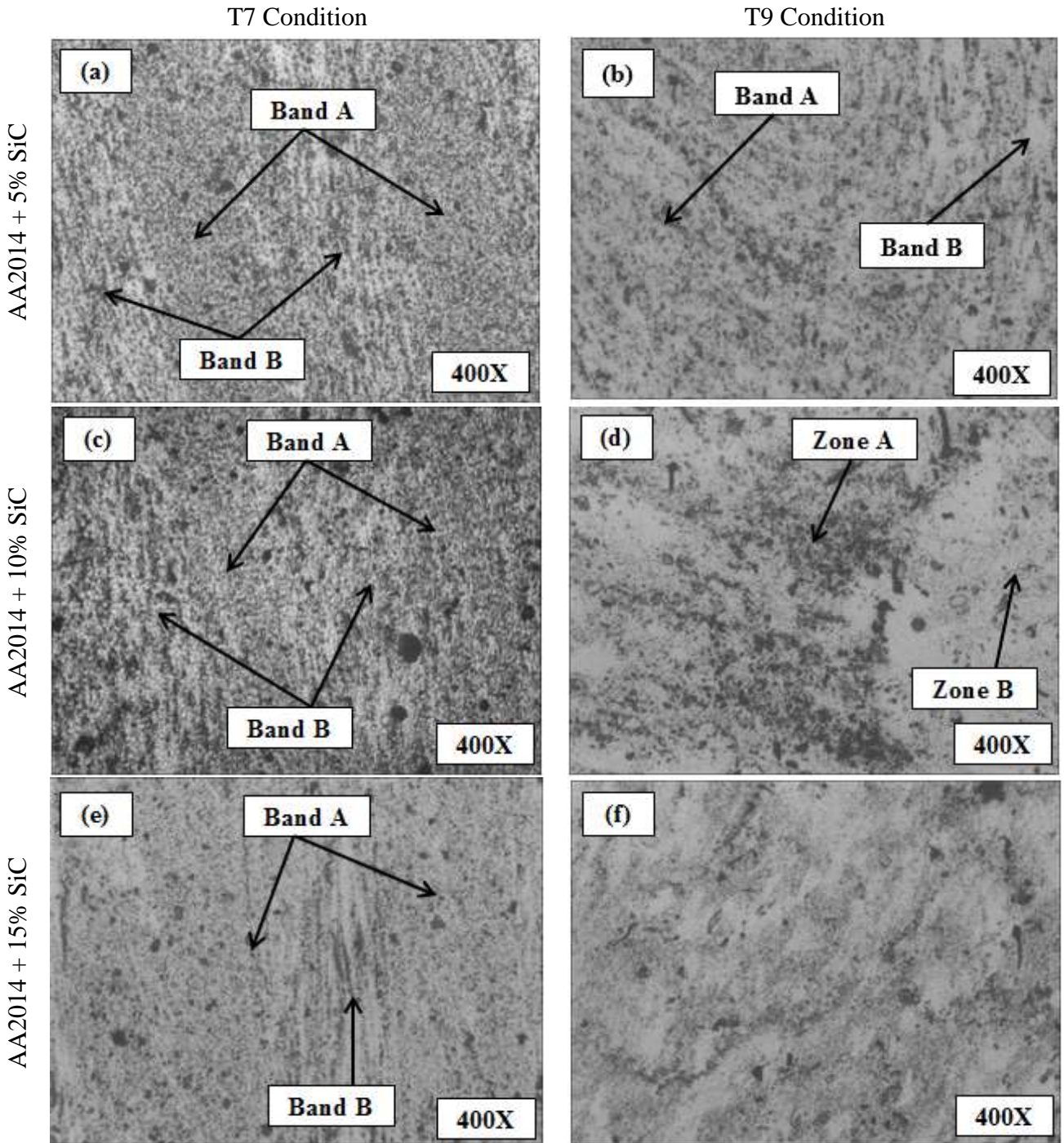
Figure 4.8 Micrographic images from NZ of AA 2014 + 5%, 10% and 15% SiC processed at T7 and T9 condition
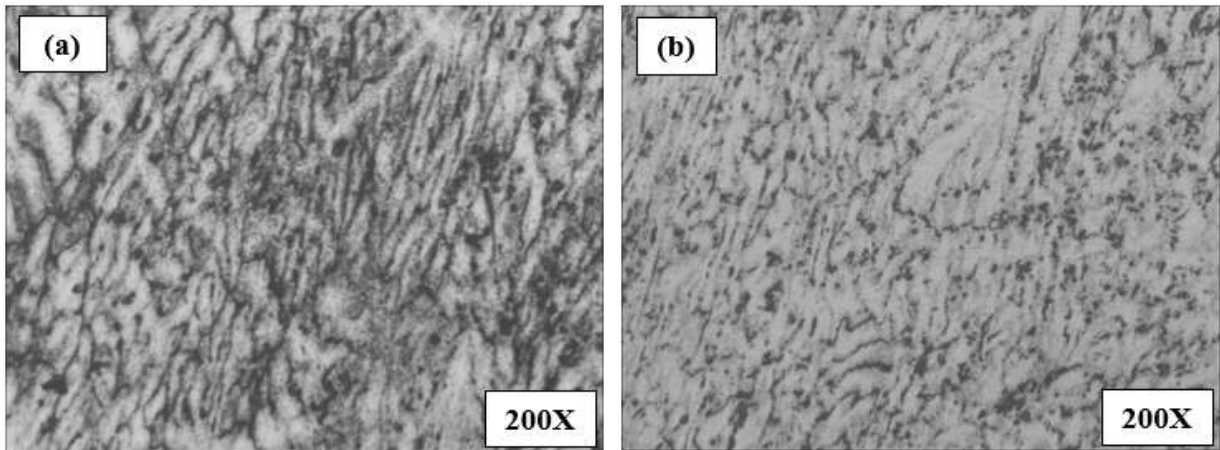
Figure 4.9 Optical micrographs from TMAZ of AA 2014 + 5% SiC (a) T7 condition and (b) T9 condition

The micrographs of the transition zone of AA 2014 + 10% SiC processed under both conditions is shown in Figure 4.10. It can be observed that for T9 processed composites, the interface of NZ and TMAZ shows the presence of few agglomerations of SiC particles. However, the same interface for T7 processed specimens showed the presence of fine and elongated SiC particles. The presence of agglomeration/clusters of reinforcement particles interface was attributed to lower tool rotational speed. It should be noted that lower tool rotational speed will result in the improper flow of plasticized material. On the other side, higher rotational speed will tend to break the SiC particles present in the matrix of aluminium. Thus, it can be said that a lower rotational speed of 190 rpm will not generate the enough stirring action required to break the clusters of SiC particles present in the matrix. Due to the same, agglomerated SiC particles can be observed at the interface of NZ and TMAZ for T9 processed specimens. In contrast, the higher rotational speed of 270 rpm generates the necessary stirring action. Not only this, higher rotational speed will break the clusters of SiC particles and distribute the broken SiC particles at the interface of NZ and TMAZ. At the same time, it should be noted that higher rotational speed results in a higher heat generation. Due to higher rotational speed, the particles tend to travels from plastically deformed softened NZ towards TMAZ. However, the temperature difference between NZ and TMAZ restricts the motion of particles. Thus, the orientation of particles on the NZ/TMAZ interface can be observed. Similar results were reported by Rana and Badheka, (2019). Apart from this, it is evident from Figure 4.10 that T7 processed composite has a larger area of TMAZ compared to T9 processed specimens. Thus, it can be said that increasing the rotational speed from 190 rpm to 270 rpm tends to increase the area cover by TMAZ. Rana and Badheka, (2018)

observed asymmetric distribution of B$_4$C particles and reported a higher number of agglomeration of B$_4$C particles on the AS of composite. However, increasing the number of passes and changing the tool transverse direction was found to be beneficial towards the reduction of agglomeration. Contradictory to this, in the present study, no such agglomeration of reinforcement particles was observed on AS of all processed composites. In the earlier case, reinforcement particles were externally introduced in the matrix and surface composites were manufactured. With reference to surface composites, the material flow generated by the rotating tool is such that the reinforcement particles travel with plasticize material and get embedded in the matrix. Whereas in the present study, reinforcement particles were already present in the aluminium matrix, as bulk composites were manufactured using the stir casting process. Thus in the case of bulk composite, the rotating tool will tend to break the agglomeration of reinforcement particles, refine them and distribute the refined reinforcement particles in plasticized material. Similar observations were made for other as-cast composites.

The NZ/TMAZ interface at higher magnification for AA 2014 + 15% SiC processed by both conditions is shown in Figure 4.11. Arrows are shown in Figure 4.11(a) and (b) represent the presence of SiC particles at the NZ/TMAZ interface. While comparing Figure 4.11(a) with (b), it can be observed that the interface of composite processed by T9 condition shows a higher amount of SiC particles compared to T7 processed composite. Apart from this, the interface of T7 processed composite evident grain refinement and uniform distribution of SiC particles. Whereas, T9 processed composites were found to have densification of larger grains of SiC particles along with few clusters. It should be noted that an increase in transverse speed will tend to reduce the size of SiC particles. In the same line, when transverse speed was an increase from 50 mm/min to 78 mm/min, refinement in SiC particles can be observed. Thus compared to T9 processed specimens, a smaller grain size of SiC particles can be observed in T7 processed specimens.
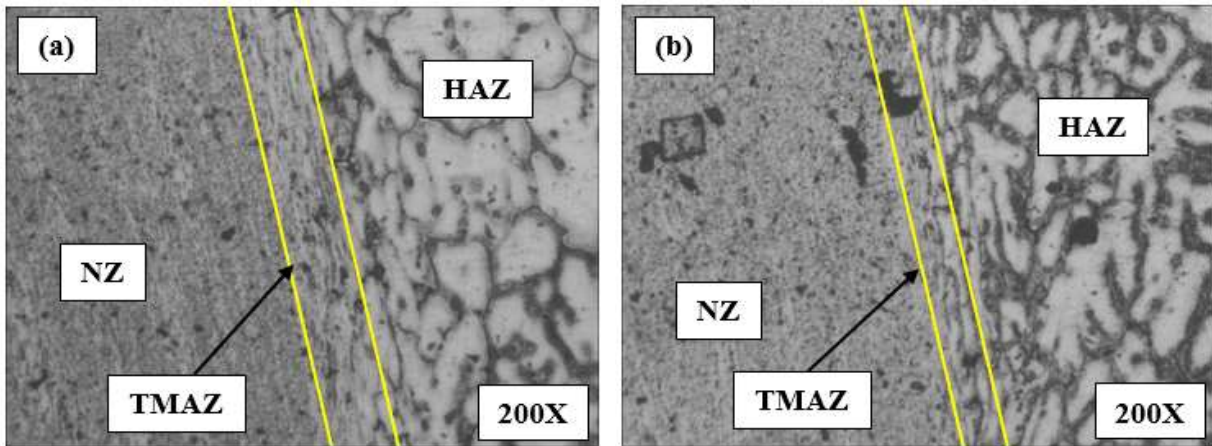
Figure 4.10 Optical micrographs from transmission zone of AA 2014 + 10% SiC (a) T7 condition and (b) T9 condition
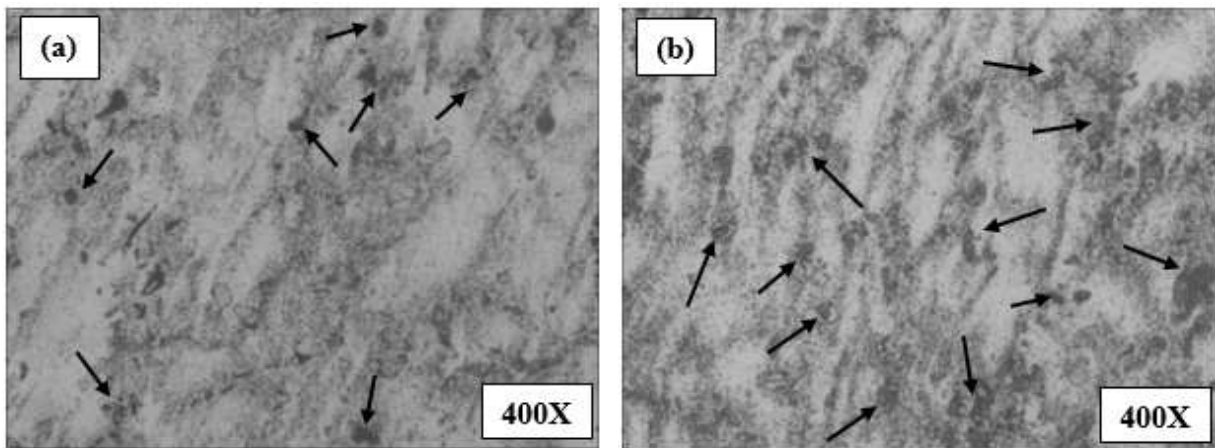

Figure 4.11 Micrographs of NZ/TMAZ interface of AA 2014 + 15% SiC (a) T7 condition and (b) T9 condition

4.5.2 Comparative study between as-cast and processed composites

The microstructure of as-cast composites with TMAZ and NZ of AA 2014 + 5%, 10% and 15% SiC processed at T7 and T9 conditions is shown in Figure 4.12. As discussed earlier, material under HAZ will only experience the thermal history and will not undergo deformation. Thus, HAZ was found to have a dendritic like structure (Figure 4.12(b), (k) and (q)) which were similar to the microstructure of the as-cast composite. It should be noted that in the microstructure of HAZ, the recrystallization effect can be visible from the size of grains. At the same time, the orientation of grain can be observed towards TMAZ, which is due to the thermomechanical effect experienced during FSP (John, Shanmuganatan, Kiran, Senthil Kumar, & Krishnamurthy, 2019). Owing to the elevated temperature which was retained for a longer period, the appearance of enlarged

92

grains can be observed in HAZ (Astarita, Squillace, & Carrino, 2014). While comparing microstructures of as-cast composites with NZ, a subsequent reduction in grain size can be observed for all processed composites. It should be noted that the shoulder of the FSP tool will generate the necessary frictional heat which will lead to plastic deformation of material present below the shoulder. Along with this, the pin of the FSP tool while rotating tends to break the SiC particles present in the aluminium matrix. Thus, the rotation of the tool will tend to break the SiC particles and distributes them uniformly in NZ of processed composites. Also, while comparing Figure 4.12(g) and (i), the voids which were initially present in as-cast composites were no longer visible in NZ of processed composites. The possible reason for this could be the rotation of the tool which will deform material plastically. The flow of this plasticized material will tend to fill the voids and other casting defects present in as-cast composites. Thus, NZ along with TMAZ of composite (Figure 4.12(h) and (i)) was found to have defect free microstructure. Similarly, the microstructure of as-cast AA 2014 + 15% SiC showed the presence of few voids (Figure 4.12 (m)) which were ultimately found resolved in TMAZ and NZ (Figure 4.12(n) and (o)). While comparing Figure 4.12(a) – (c) it can be observed that HAZ and NZ of the processed AA 2014 + 5% SiC were found to have few voids even though the as-cast composite not having any defects. The average grain size of as-cast composites were 61.95 μm, which was found to reduce in NZ of T7 processed AA 2014 + 5%, 10 % and 15% SiC composites to 5.45 μm, 5.50 μm and 7.75 μm respectively. Thus, it can be said that the stirring action of the tool has played a crucial role in grain refinement. It is a known fact that grain refinement acts towards the enhancement of the mechanical properties of processed composites.

Nevertheless, T9 processed specimens showed the presence of few voids in NZ. For instance, while comparing Figure 4.12(d), (e) and (f) it can be observed that TMAZ and NZ of the processed composites were found to have few voids. The possible reason for this defect in NZ could be processing parameters, especially rotational speed and transverse speed. Lower rotational speed will generate an insufficient flow of plasticized material. This lack of material flow will result in the formation of defects or will be unable to vanish the casting defected which were already present in as-cast composites. At the same time, lower transverse speed will result in excessive heat generation along with improper processing. Thus, lower transverse speed will result in poor processing and due to which more porosity and defects can be observed. Therefore, composites

processed with a combination of lower rotational speed and lower transverse speed was found to have few defects in NZ and TMAZ. Similar results were observed for T9 processed AA 2014 + 15% SiC composites. From Figure 4.12 (p), (q) and (r) it can be observed that even after processing still few voids that were present in HAZ, TMAZ and NZ. Along with this, few agglomerated SiC particles can also be observed in NZ. Similarly, while comparing Figure 4.12 (j) and (k) it can be observed that as-cast composites were having few voids which were still present in HAZ even after processing. However, TMAZ and NZ were found to have defects free structures along with few agglomerations/clusters of SiC particles in NZ (Figure 4.12(l)). It should be noted that clusters of reinforcement particles adversely affect the mechanical properties of resulting processed composites. Post processing by T9 condition, the average gain size in NZ of AA 2014 + 5%, 10% and 15% SiC composites were found to reduce from 61.95 µm to 7.75 µm, 9.20 µm and 7.90 µm. Owing to the clusters of SiC particles observed in Figure 4.12(l), T9 processed AA 2014 + 10% SiC was having a maximum average grain size of 9.20 µm. A combination of lower rotational speed and lower transverse speed might not generate enough thrust which is required to break agglomeration of SiC particles or SiC particles. As a result of which, few agglomerations of SiC particles can be observed in NZ and TMAZ. Also due to this, T9 processed composite was found to have a higher grain size in NZ when compared to the average grain size of T7 processed composites.
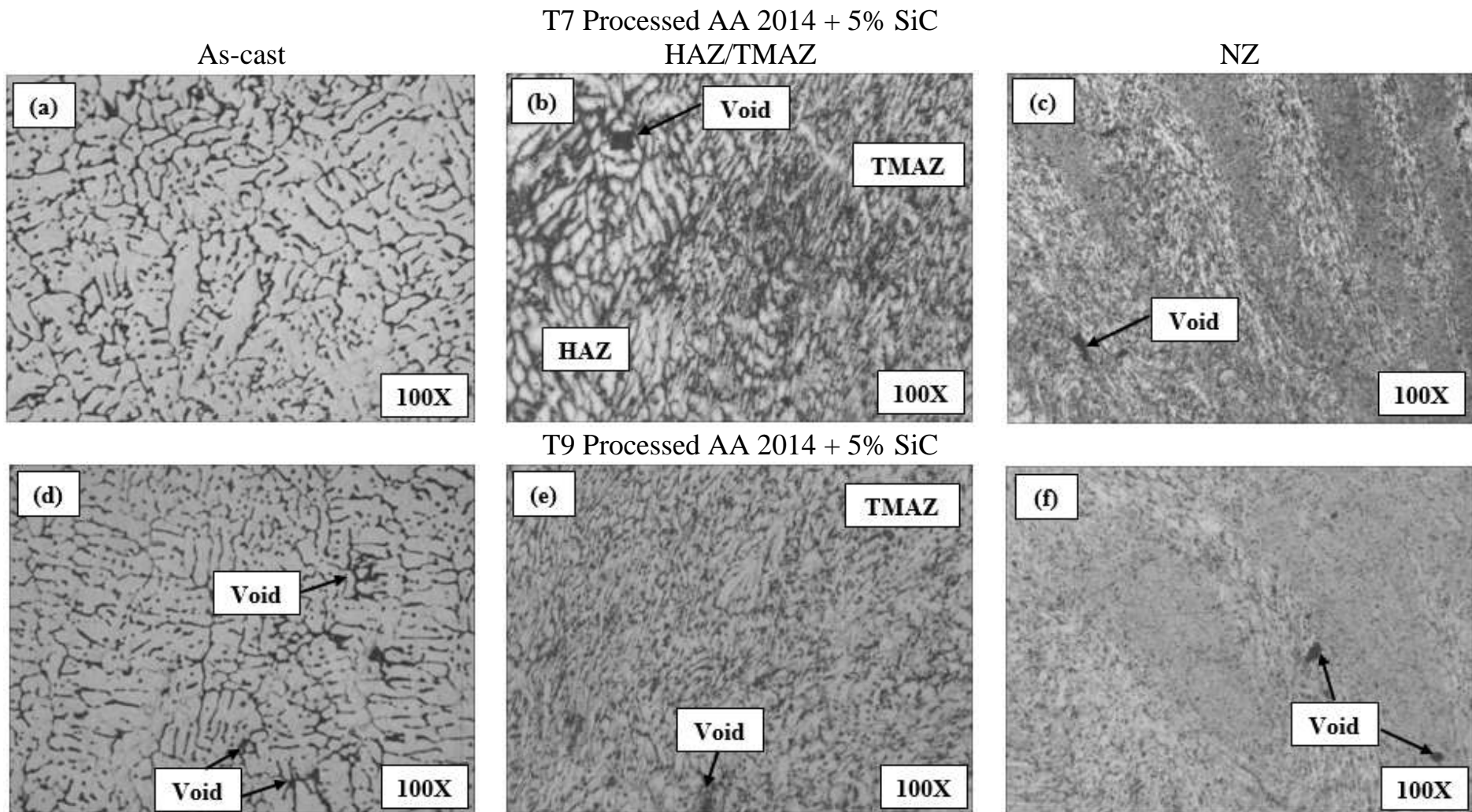
T7 Processed AA 2014 + 5% SiC

As-cast · HAZ/TMAZ · NZ

Figure 4.12 Comparison between micrograph of as-cast composite and FSPed composites (Cont.)

T7 Processed AA 2014 + 10% SiC

As-cast   HAZ/TMAZ   NZ

T9 Processed AA 2014 + 10% SiC

Figure 4.12 Comparison between micrograph of as-cast composite and FSPed composites (Cont.)

T7 Processed AA 2014 + 15% SiC

As-cast   HAZ/TMAZ   NZ
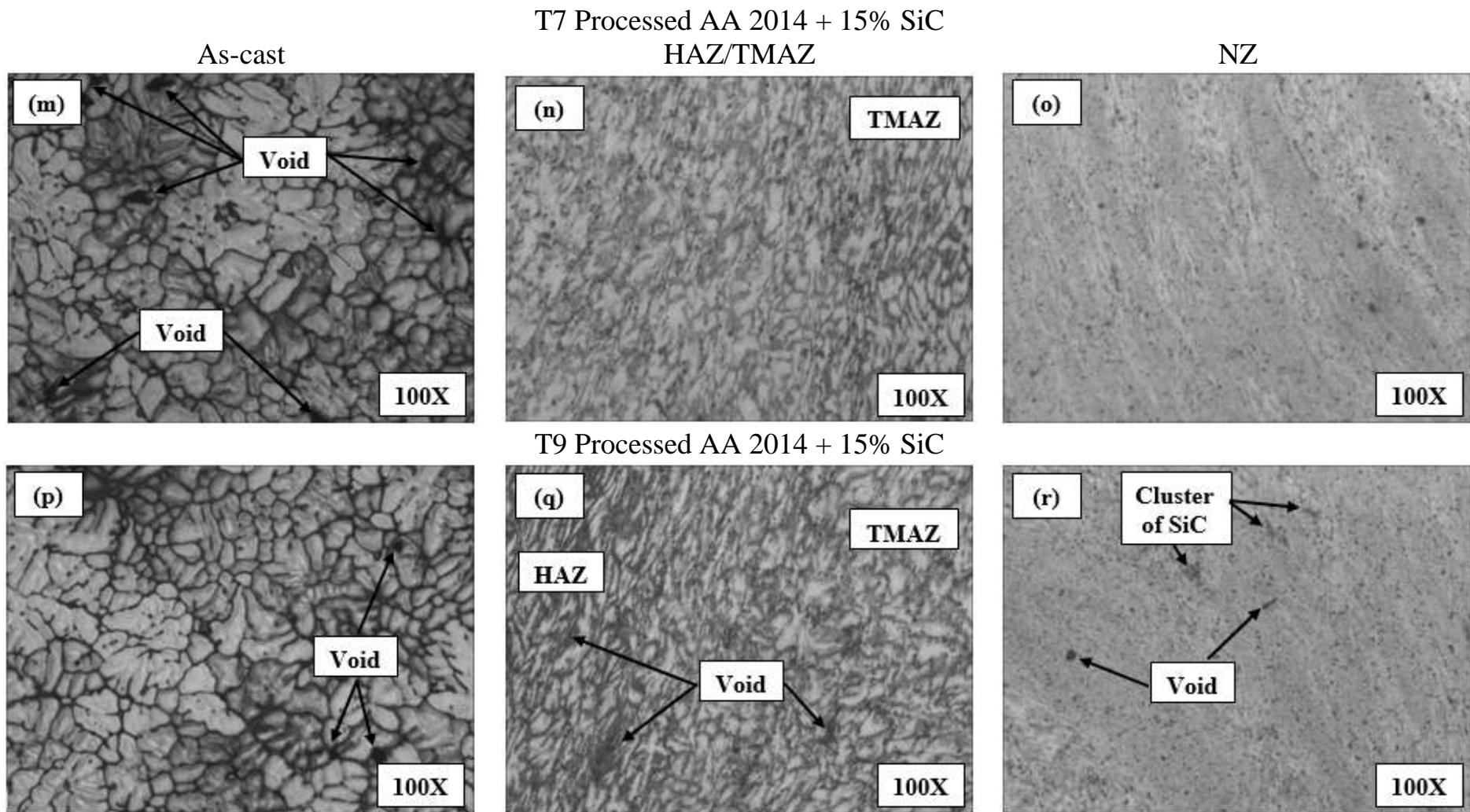
T9 Processed AA 2014 + 15% SiC

Figure 4.12 Comparison between micrograph of as-cast composite and FSPed composites

97
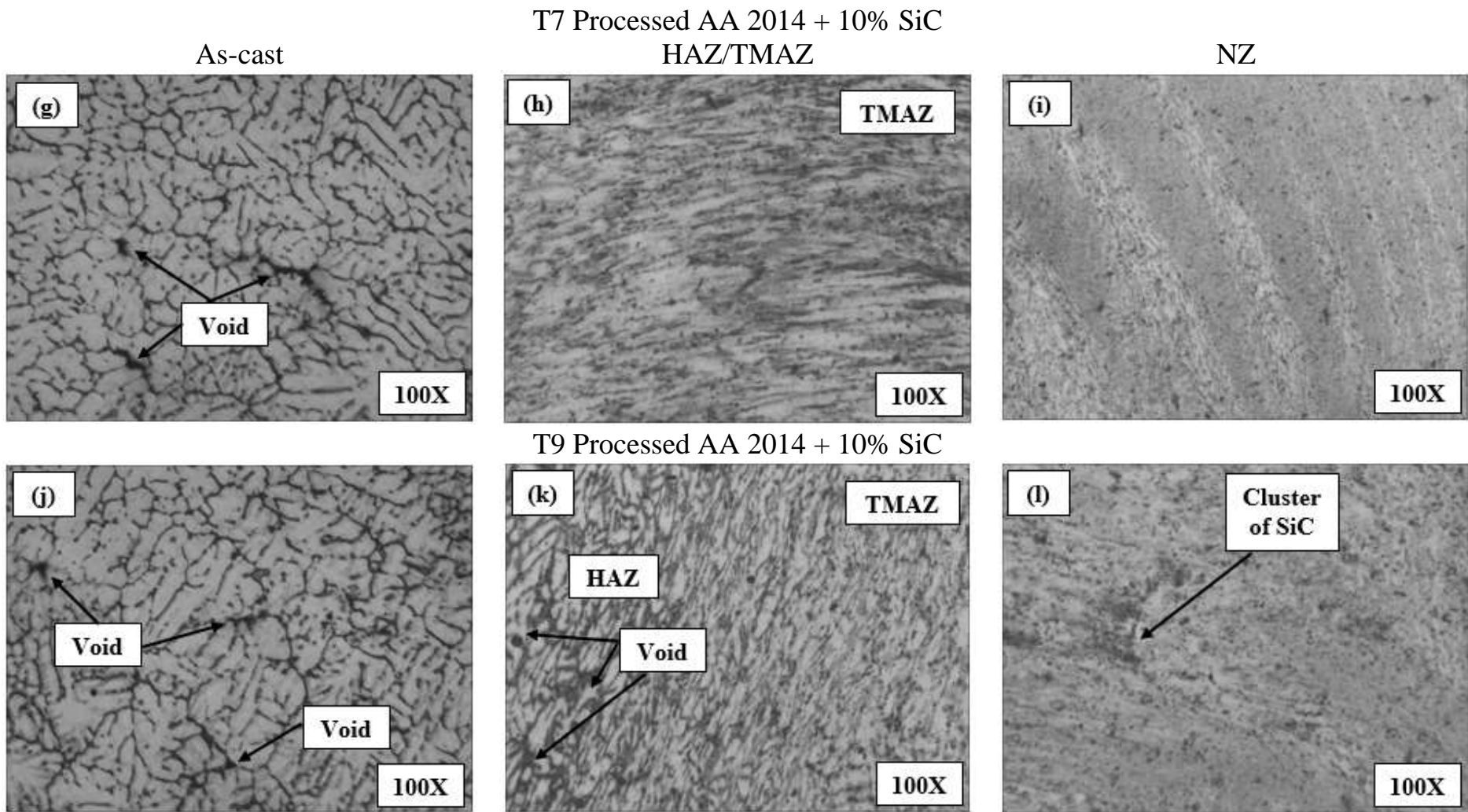
4.5.3 Microhardness Comparison between as-cast and processed composites

As mentioned earlier, a microhardness test was conducted on as-cast and processed composites. The plots of microhardness of as-cast, T7 processed and T9 processed composite is shown in Figure 4.13. The microhardness was measured along the vertical direction in NZ starting from bottom surface to top surface. From the plot shown in Figure 4.13(a), it can be observed that the variation in microhardness of as-cast and processed specimens along the thickness is almost negligible. This negligible variation in microhardness indeed indicates the homogeneous distribution of SiC particles in the aluminium matrix. Similar observation can also be made for other two composites i.e. AA 2014 + 10% and 15% SiC (Figure 4.13(b) and (c)). As mentioned in the previous chapter the microhardness plot of as-cast composites showed the presence of few hikes. However, it should be noted that these hikes were absent in the microhardness plot of processed composites. At 1.5 mm above the bottom surface, the microhardness for T7 and T9 processed AA 2014 + 5% SiC composites were found to reduce from 99.6 Hv to 80.5 Hv and 76.2 HV respectively. These values were nearer to the values obtained at adjacent points and thus no hike was reported. Similar to this, the hike present at 3.5 mm above the bottom surface was no longer visible in T7 and T9 processed composites. At the same location, the microhardness of T7 and T9 processed composites was found to reduce from 106.9 Hv to 84.1 Hv and 77.7 Hv respectively. This clearly indicates that the FSP of composites tends to break the agglomeration of SiC particles which were earlier present in as-cast composites.

Similarly, post processing the dips present in Figure 4.13(a) was no longer visible. The microhardness corresponding to dip was found to increase from 72.8 Hv to 87.1 Hv and 84.1 Hv for T7 and T9 processed AA 2014 +5% SiC respectively. Similarly, two dips that were present in as-cast AA 2014 + 10% SiC were no longer visible and microhardness corresponding to those dips were found to increase from 70.8 Hv and 74.6 Hv to 90.5 Hv and 103.5 Hv respectively for T7 processed composites. However, FSP by T9 condition was unable to resolve these dips. Corresponding to the first dip microhardness of T9 processed composite was found to increase 70.8 Hv to 74.5 Hv. Whereas, corresponding to second dip microhardness was found to reduce from 74.6 Hv to 69.1 Hv. As reported in Figure 4.8(d), the microstructure of T9 processed AA 2014 + 10% SiC was found to have particles rich and particle deficient regions. Due to the

particle deficient region present in T9 processed composites, the dip present in as-cast composites was unable to resolve and a further reduction in microhardness was reported. While observing Figure 4.13(c), it can be observed that both the dips which were initially present in as-cast composites were no longer present post FSP. The microhardness corresponding to two dips was 71.6 Hv and 53.9 Hv which were found to increase to 86.4 Hv and 86.5 Hv for T7 processed composites and 79.5 Hv and 84.2 Hv for T9 processed composites. These enhancements in microhardness and disappearance of previously observed dips, straight forward indicate that FSP tends to resolve casting defects and attempts to embed reinforcement particles in particle free regions.

The average microhardness of as-cast, T7 processed and T9 processed composites is shown in Figure 4.14. Apart from T7 processed AA 2014 + 10% and 15% SiC, the rest of all composites revealed a reduction in microhardness post processing. Due to casting defects, the initial hardness of as-cast composites was lower and as reported in microstructure, FSP tends to fill the voids and avoids defects present in as-cast composites. As an attribute to this, enhanced hardness of T7 processed AA 2014 +10% and 15% SiC was reported. As reported in Figure 4.12(c), few voids were still present in NZ of AA 2014 + 5% SiC even after T7 processing. Along with this, from Figure 4.8(a) it was observed that NZ was characterised by two different bands having different shapes and sizes of SiC particles. Owing to these two reasons, a reduction in microhardness of T7 processed AA 2014 + 5% SiC was observed. Among all T7 processed composites, the highest microhardness of 88.56 Hv was observed for AA 2014 + 10% SiC. The highest microhardness was attributed to nearly linear distributions of microhardness plotted in Figure 4.13(b).

The average microhardness of all T9 processed composites was found to degrade when compared to as-cast composites. As shown in Figure 4.14, the microhardness of T9 processed AA 2014 + 5%, 10% and 15% SiC composites was found to decrease from 85 Hv, 86.35 Hv and 86.18 Hv to 75.36 Hv, 75.25 Hv and 81.98 Hv respectively. As represented in Figure 4.12 (f), (l) and (r), NZ of T9 processed was found to have few voids or agglomeration of SiC particles. The presence of voids tends to reduce the microhardness of processed composites. Apart from this, agglomerated SiC particles indicate that there exists the possibility of particle deficient region due to lack of stirring. Due to the same, a reduction in hardness was reported. Nevertheless, an almost linear

distribution of microhardness without many hikes and dips resulted in the highest microhardness of 81.98 Hv in NZ of AA 2014 + 15% SiC.
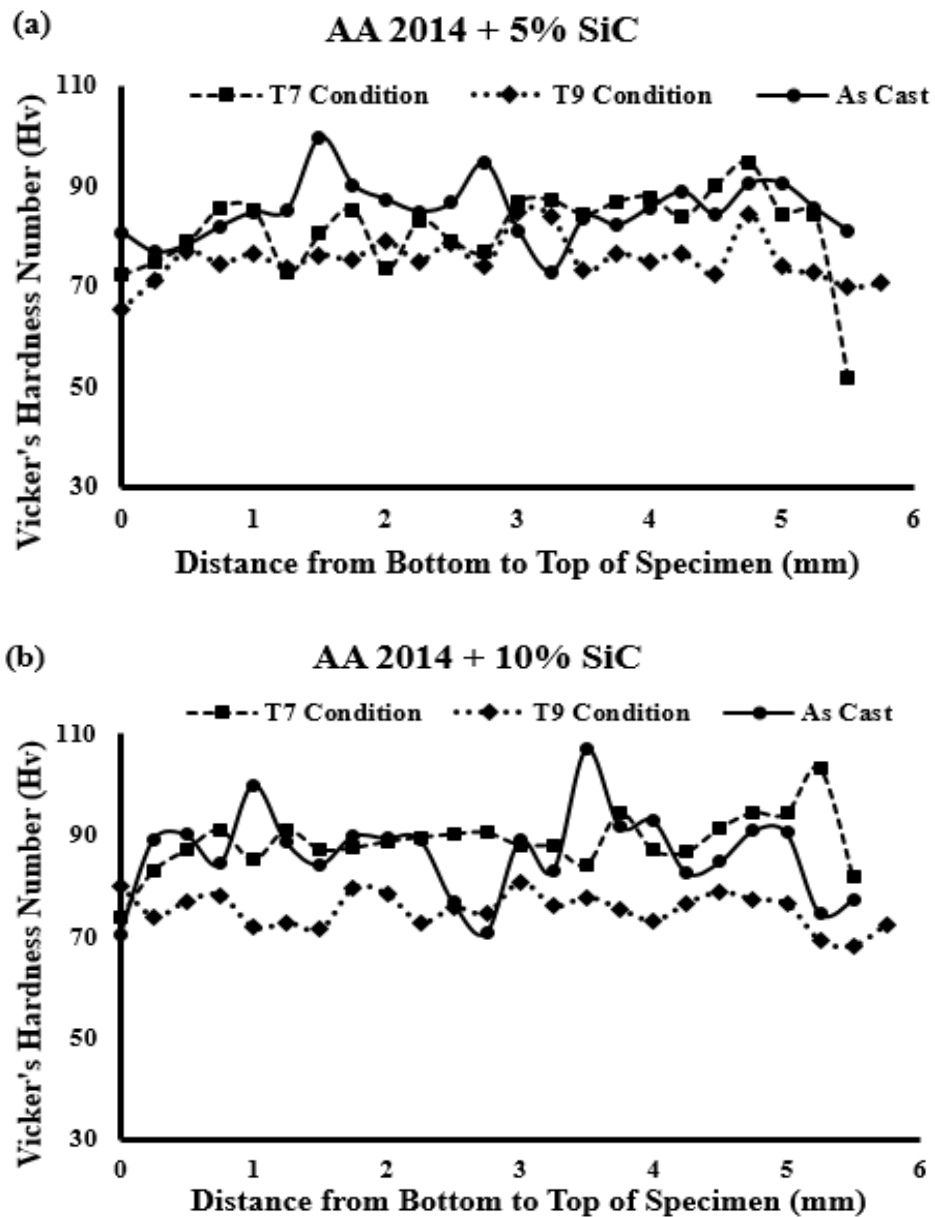

Figure 4.13 Plot of microhardness of as-cast and processed composites (a) AA 2014 + 5% SiC, (b) AA 2014 + 10% SiC and (c) AA 2014 +15% SiC (cont.)
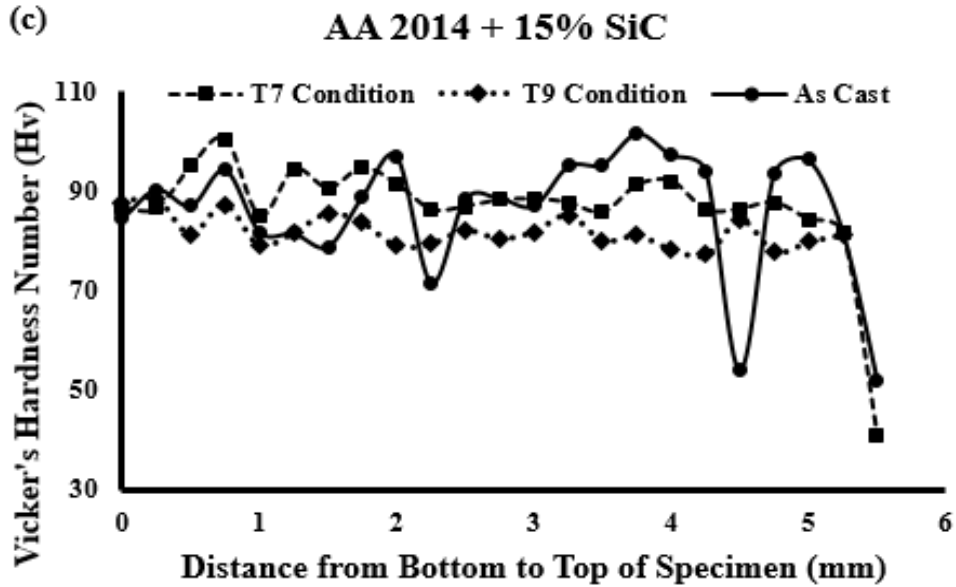
Figure 4.13 Plot of microhardness of as-cast and processed composites (a) AA 2014 + 5% SiC, (b) AA 2014 + 10% SiC and (c) AA 2014 +15% SiC

From Figure 4.14, it can be observed that T9 processed composites were found to have the lowest average microhardness. As reported earlier, T9 processed composites were having a higher grain size compared to T7 processed composites. It is a known fact that grain refinement plays a crucial role in the enhancement of microhardness properties. Thus, due to the lower grain size of T7 processed composites, higher microhardness was reported. Other than this, the obvious reasons for the reduction in microhardness were voids, agglomeration of SiC particles and particles free region. Also, process parameters play a critical role on the resulting microhardness of composites. As reported earlier combination of rotational speed of 190 rpm and transverse speed of 50 mm/min will result in improper stirring. Due to the same, processing defects were visible in NZ of T9 processed composites. Along with this, lower transverse speed will tend to generate higher frictional heat. It is a well-known fact that higher heat generation will result in the dissolution of several strengthening precipitates. Due to the dissolution of strengthening precipitates, reduction in average microhardness was observed for T9 processed composites. On the other side, the combination of the higher rotational speed of 270 rpm and higher transverse speed of 78 mm/min has proven to be beneficial towards the improvement of average hardness. This clearly indicates that processing parameters of the T7 condition have resulted in appropriate stirring action. Due to the same, higher average microhardness can be observed for T7 processed composites compared to T9 processed composites.
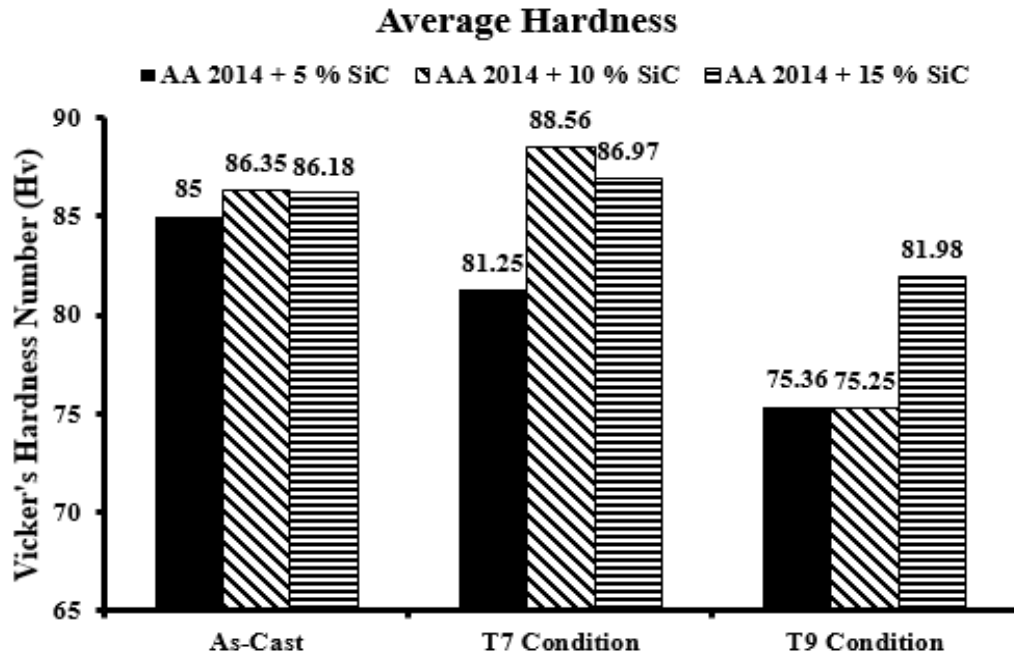
Figure 4.14 Plot of average microhardness of as-cast and processed composites

4.6 Tribological Investigation

To investigate tribological properties of processed composites and compare the results with that of as-cast composites, the wear test was performed on a pin-on-disc setup. The pin required for the wear test was cut using a wire cut Electrical Discharge Machine (EDM). To get a better idea about wear properties, the pin required for the wear test was carefully cut from the NZ of processed composites. The dimension of the pin which was extracted from NZ of processed composites is shown in Figure 4.6. The testing procedure, loading condition, sliding distance and other parameters of the wear test were similar to that mentioned in section 3.3.4.

4.6.1 Comparison of Wear Characteristic of processed and as-cast composites

The change in weight of as-cast, T7 processed and T9 processed wear specimens are tabulated in Table 4.2. While referring to the variation in the mass of specimens in Table 4.2, it can be observed that loss of weight for processed composites is comparatively lower than that of as-cast composites (except AA 2014 + 15% SiC). Thus, it can be said that FSP will tend to alter the microstructural properties which will enhance the wear resistance and thus reduces the weight loss of the processed composites. Apart from this,

it should be noted that the loss in weight of T7 processed specimens is comparatively lower than the loss in weight of T9 processed composites.

Table 4.2 Comparison of change in mass of as-cast, T7 processed and T9 processed wear specimens

As-cast			T7 processed			T9 processed		
Initial Weight (g)	Final Weight (g)	Δ W (g)	Initial Weight (g)	Final Weight (g)	Δ W (g)	Initial Weight (g)	Final Weight (g)	Δ W (g)
AA 2014 + 5% SiC								
0.447	0.432	0.015	0.41	0.4	0.01	0.449	0.436	0.013
AA 2014 + 10% SiC								
0.41	0.399	0.011	0.424	0.42	0.004	0.423	0.421	0.002
AA 2014 + 15% SiC								
0.415	0.414	0.001	0.423	0.417	0.006	0.403	0.392	0.011

A comparative plot showing the variation in wear of as-cast, T7 processed and T9 processed AA 2014 + 5% SiC composites with respect to sliding distance is shown in Figure 4.15. From Figure 4.15, it can be observed that the wear of processed as well as as-cast composites increases with the increase in sliding distance. As reported earlier that the wear plot of as-cast AA 2014 + 5% SiC was found to have three different phases i.e. Phase 1, Phase 2 and Phase 3. In the same line, T7 processed AA 2014 + 5% SiC also revealed Phase 1, where the wear of processed composite increases rapidly with the initial increase in sliding distance (upto 200 m). The reasons behind the higher wear rate during Phase 1 have already been discussed earlier. Apart from this, it should be noted that the detachment of loosely hold reinforcement particles and other hard matter from the aluminium matrix will result in higher wear during the initial few meters of sliding distance (Shaik, Sudhakar, Bharat, Varshini, & Vikas, 2020). However, with the further increase in sliding distance, the wear of processed composites increases gradually. It should be noted that it was difficult to differentiate the Phase 2 and Phase 3 in wear plot of T7 processed AA 2014 + 5% SiC. On the other side, the wear plot of T9 processed AA 2014 + 5% SiC didn't reveal any phases. A continuous increase in wear of T9 processed AA 2014 + 5% SiC can be observed with the increase in sliding distance. Irrespective of the processing condition, the wear of processed AA 2014 + 5% SiC was lower than that observed for the as-cast composite. As reported earlier, FSP of composites leads to grain refinement, distributes SiC particles more homogenously, reduces casting defects and

reduces the irregularities/asperities at the microscopic level. Due to this, enhancement in wear properties/wear resistance of processed composites can be observed. Apart from this, it has been reported that FSP reduces the detachment of reinforcement and matrix material from the surface in the form of wear debris and thus lower wear of processed composites can be observed (Barati, Abbasi, & Abedini, 2019).
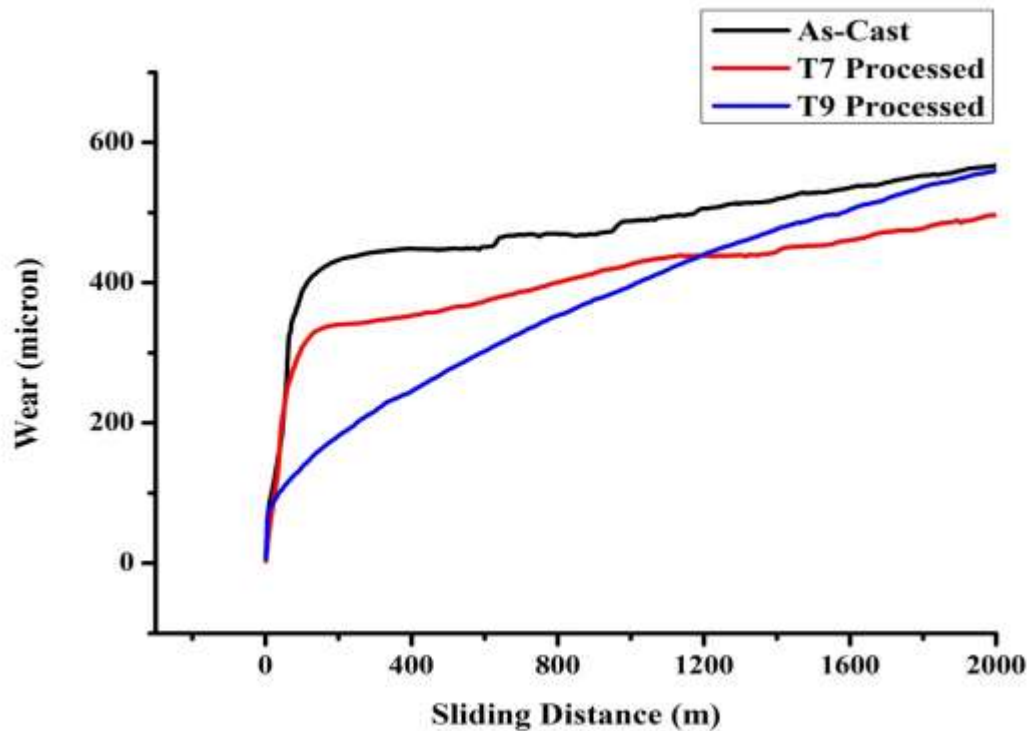

Figure 4.15 Wear plot of as-cast, T7 processed and T9 processed AA 2014 + 5% SiC

The wear plot for as-cast, T7 processed and T9 processed AA 2014 + 10% SiC is shown in Figure 4.16. It can be observed that the phases which were witnessed for as-cast AA 2014 + 10% SiC were no longer present in the wear plot of T7 and T9 processed composites. The wear plot showcases that the wear of processed composite increases continuously with respect to sliding distance. Similar to Figure 4.15, wear of processed AA 2014 + 10% SiC composites were comparatively lower than that of as-cast. The reason for the same has been discussed earlier. While comparing the wear of as-cast, T7 processed and T9 processed AA 2014 + 15% SiC, an unusual result was observed. From Figure 4.17 it can be observed that T9 processed composite was having the highest wear compared to T7 processed composites and as-cast composites. The possible reason for this could be the presence of agglomeration of SiC particles and void formation in T9 processed specimens. Another possible reason for this could be the transformation of

wear behavior from two-body abrasion to three-body abrasion. It should be noted that the presence of SiC particles dominates the wear of processed composites. As long as the SiC particles are embedded in the aluminium matrix, the wear of processed composite will be two-body abrasive wear. As the sliding distance increases, the wear of processed composites will increase which may transform the two-body abrasive wear to three-body abrasive wear. The presence of agglomerated SiC particles could be the possible reason for this transformation of wear behavior. As long as the agglomerated SiC particles are in contact with the rotating steel disc, the wear will be comparatively lesser. As wear increases the SiC particles will get separated from the aluminium matrix and will get removed as wear debris due to abrasion wear. This will lead to direct contact of the aluminium matrix with rotating steel disc and thus increase in wear is reflected for T9 processed composites.
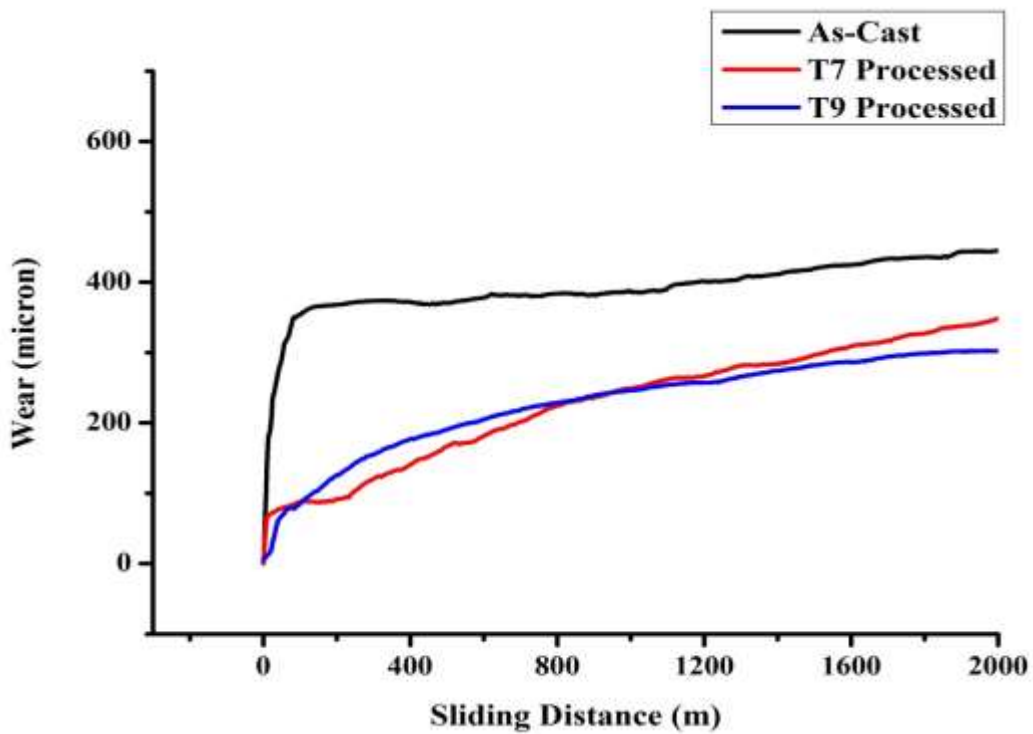

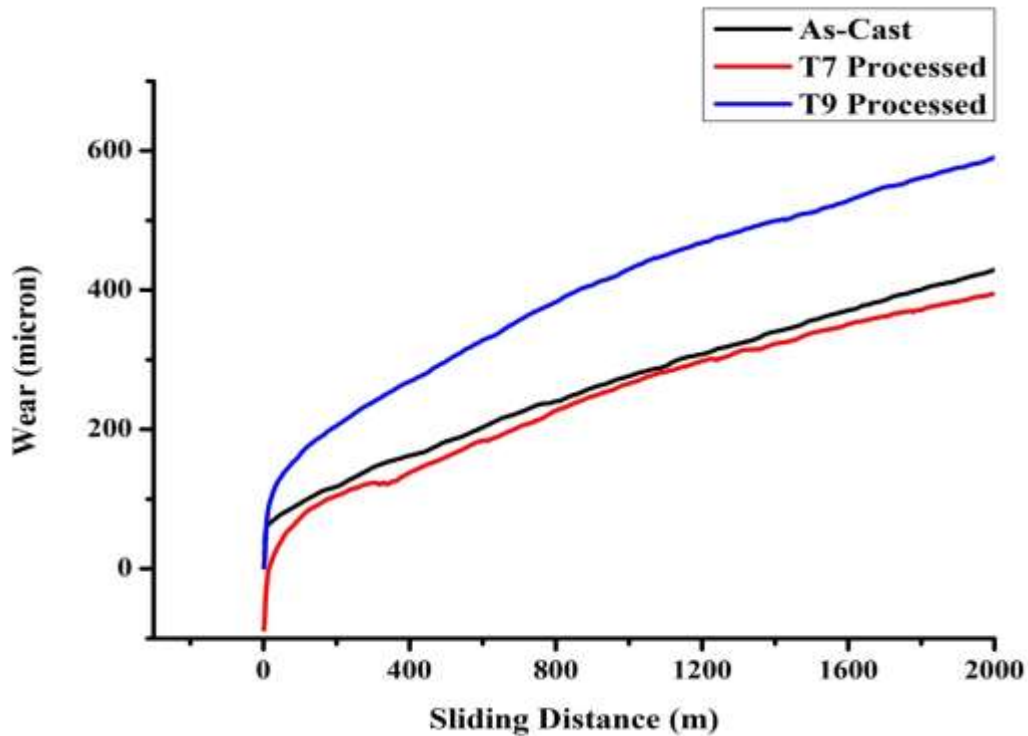Figure 4.16 Wear plot of as-cast, T7 processed and T9 processed AA 2014 + 10% SiC

Figure 4.17 Wear plot of as-cast, T7 processed and T9 processed AA 2014 + 15% SiC

The average wear of as-cast, T7 processed and T9 processed composites are shown in Figure 4.18. Except for T9 processed AA 2014 + 15% SiC, all other composites revealed a reduction in wear post FSP. With the increase in weight percent of SiC particles from 5% to 10%, the wear resistance of the processed composites was found to increase. This could be attributed to the presence of SiC particles which are hard in nature. SiC particles will provide strength to the aluminium matrix by protecting the matrix during the abrasive action of the rotating disc. It has been reported that an increase in weight percent of reinforcement beyond certain limits, will promote the three body abrasive wear and thus will increase the wear (Baradeswaran, Elayaperumal, & Issac, 2013). Due to the same, a reduction in wear resistance of processed composites can be observed with a further increase in weight percent of reinforcement particles from 10% to 15%. Thus, AA 2014 + 10% SiC was found to have the lowest wear among all processed composites under both conditions. Apart from this, it should be noted that an increase in frictional heat will ultimately result in a higher wear rate (Bowden & Tabor, 1951). The presence of a higher weight percent of reinforcement particles will increase the frictional heat during the wear test. Thus, maximum frictional heat will be generated for AA 2014 + 15% SiC and due to the same, T9 processed AA 2014 + 15% SiC revealed higher wear loss compared to the other two compositions. Other reasons such as homogenous

distribution of reinforcement particles with the presence of minimum defects and minimum agglomeration of reinforcement particles will affect the tribological properties of processed composites.

The NZ of AA 2014 + 5% SiC and AA 2014 + 15% SiC composites were either having particle free regions or the presence of voids along with few agglomerations of reinforcement particles. Due to the same, the wear resistance of these aforementioned composites was reduced. From Figure 4.18, it can be observed that the average wear of T9 processed composites was comparatively higher than that of T7 processed composites. However, while comparing the average wear of T7 and T9 processed AA 2014 + 10% SiC composites, a marginal reduction in the average wear can be observed. While relating the microhardness and wear results an unusual trend was observed. With reference to AA 2014 + 10% SiC, in Figure 4.14 subsequent reduction in average microhardness of T7 and T9 processed composites can be observed. However, with the reduction in average microhardness from 88.56 Hv to 75.25 Hv, wear of processed composites was found persistent. According to Archard's adhesive wear theory, enhancement in microhardness will ultimately improve the wear resistance (Archard J. F., 1953; Archard & W., 1956). However, this wear theory didn't hold true for the present case of processed AA 2014 + 10% SiC. Thus, it can be said that Archard's law is unable to predict the wear behavior of processed MMC. Previously, other researchers have also observed similar results (Rosenberger, Schvezov, & Forlerer, 2005; Savaskan & Bican, 2010; Baradeswaran, Elayaperumal, & Issac, 2013). For the rest of the two composites, the average wear of T9 processed composites was comparatively higher than that of T7 processed composites. From Figure 4.14, it can be observed that the average microhardness of T9 processed composites was comparatively lower than that of T7 processed composites. Due to the same, higher wear loss can be observed for T9 processed AA 2014 + 5% SiC and AA 2014 + 15% SiC composites. Similar results were previously reported by other researchers, where surface composites processed at higher rotational speed were found to have enhanced wear resistance (Bharti, Ghetiya, & Patel, 2020). As stated earlier, that the combination of the higher rotational speed of 270 rpm and higher transverse speed of 78 mm/min causes proper stirring action, reduces the grain size, distributes SiC particles homogenously and reduces/avoids the processing defects. Due to the same, enhanced wear resistance can be observed for T7 processed composites.
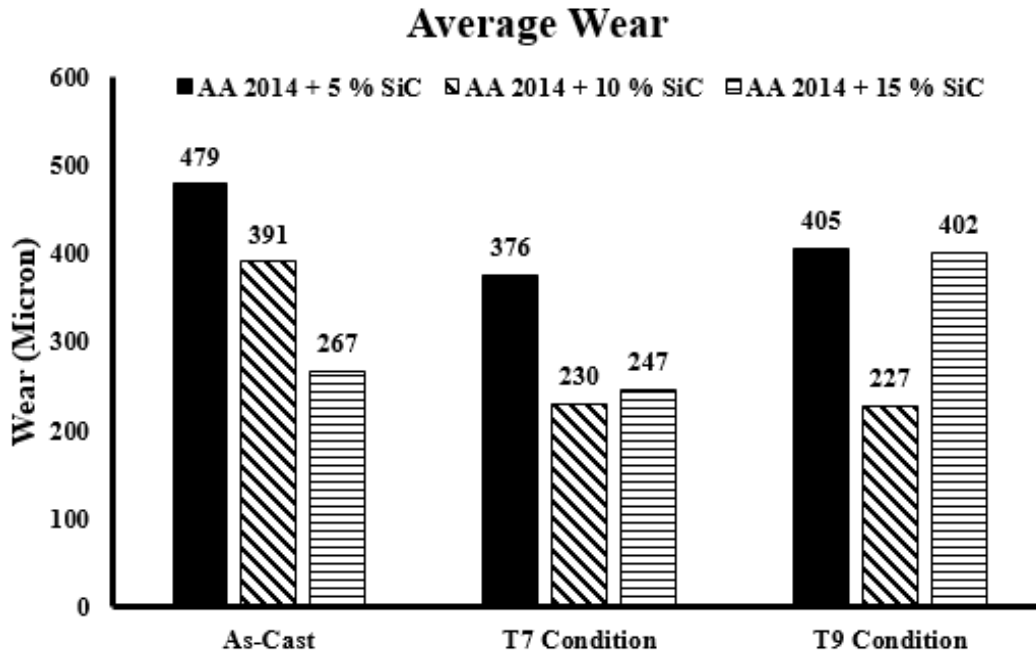
Average Wear

Figure 4.18 Average wear of as-cast, T7 processed and T9 processed composites

The variation in coefficient of friction (COF) with respect to sliding distance for all three composites is shown in Figure 4.19. For the plots of COF, it can be observed that post processing, the COF was either same as that of as-cast composites or it was increased comparatively. To get better understating, Figure 4.20 plots the average COF for all as-cast and processed composites. While comparing the plot of average wear rate and average COF, a common trend can be observed for the processed composites. An increase in the COF of processed composites was found with the increase in weight percent of SiC from 5% to 10%. Whereas, further increase in the weight percent of reinforcement particles from 10% to 15%, reduces the COF. The presence of fine and homogenously distributed SiC in the matrix of aluminium alloy will provide better wear resistance and will act as an obstacle during the wear test. Due to the same, higher frictional force/opposing force will be generated and thus increases the COF. It should be noted that the maximum COF of 0.49 and lowest wear rate of 227 microns was observed for T9 processed AA 2014 + 10% SiC.
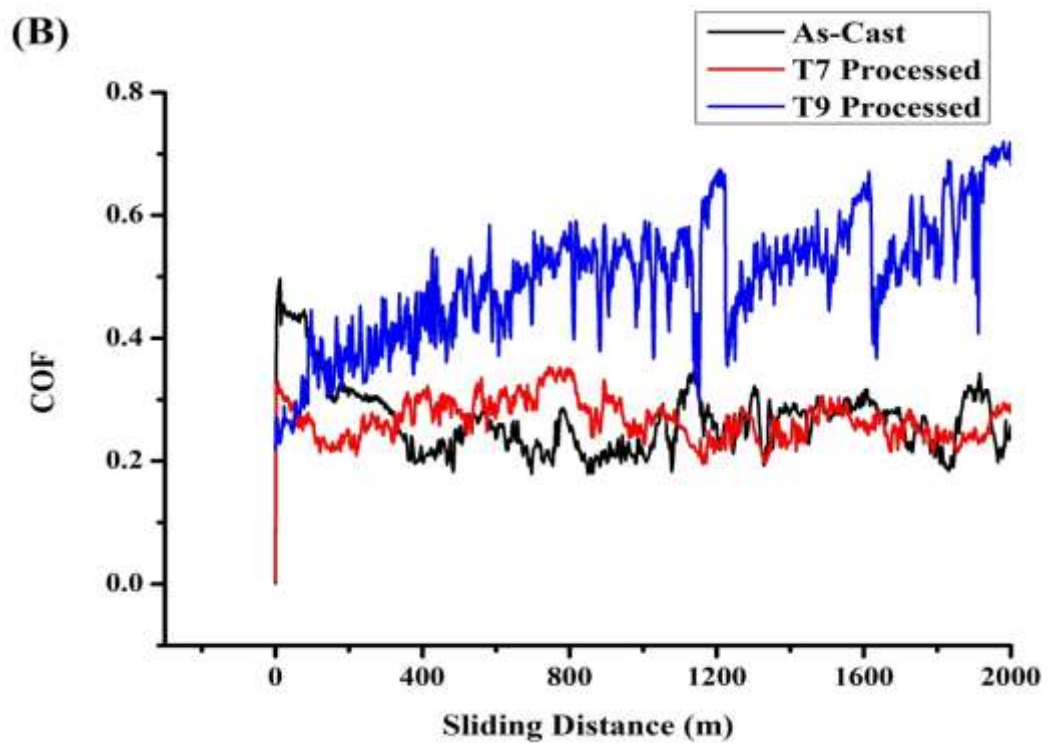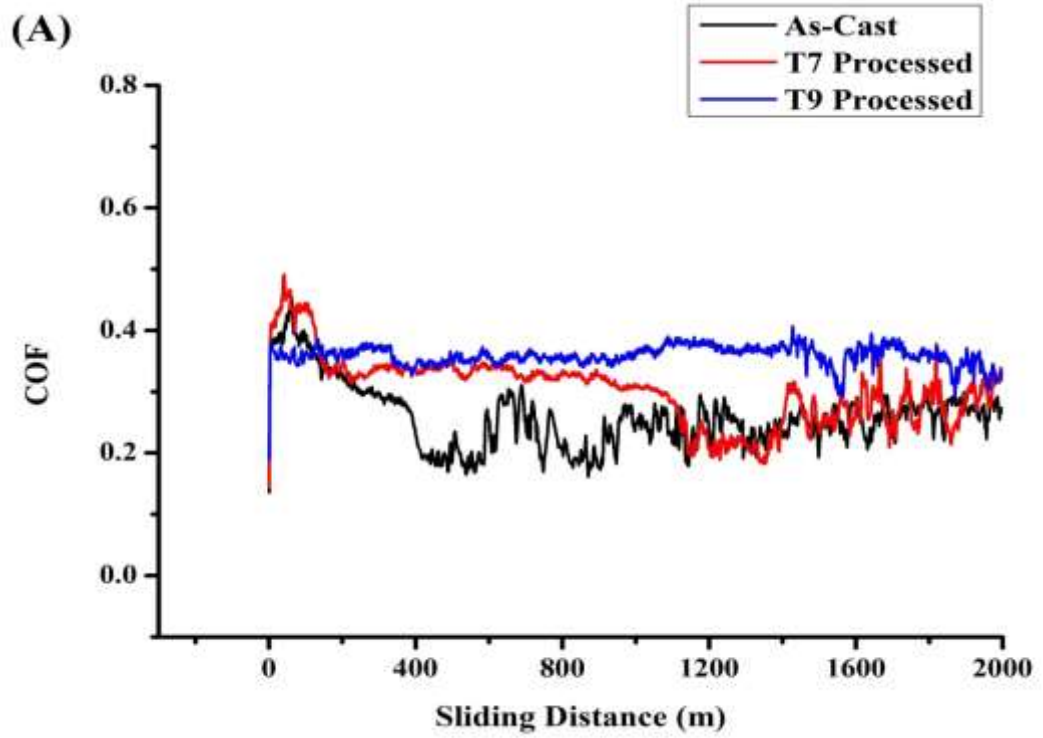
Figure 4.19 Variation in Coefficient of Friction (COF) w.r.t. sliding distance for (A) AA 2014 + 5% SiC, (B) AA 2014 + 10% SiC and (C) AA 2014 + 15% SiC (cont.)
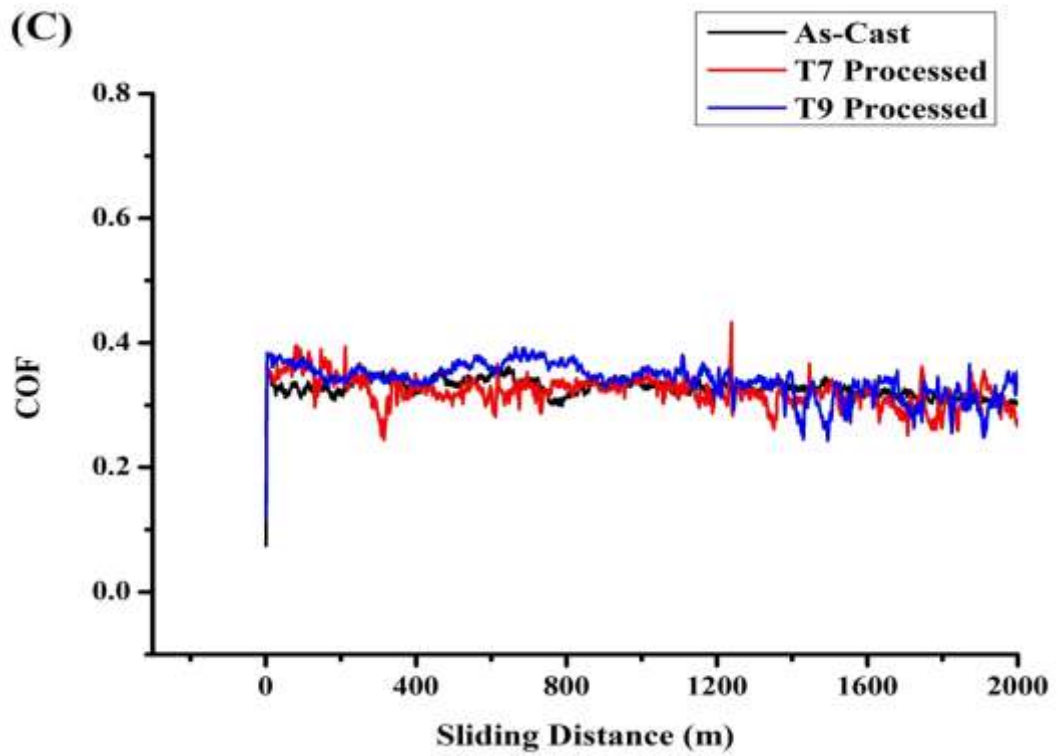
Figure 4.19 Variation in Coefficient of Friction (COF) w.r.t. sliding distance for (A) AA 2014 + 5% SiC, (B) AA 2014 + 10% SiC and (C) AA 2014 + 15% SiC
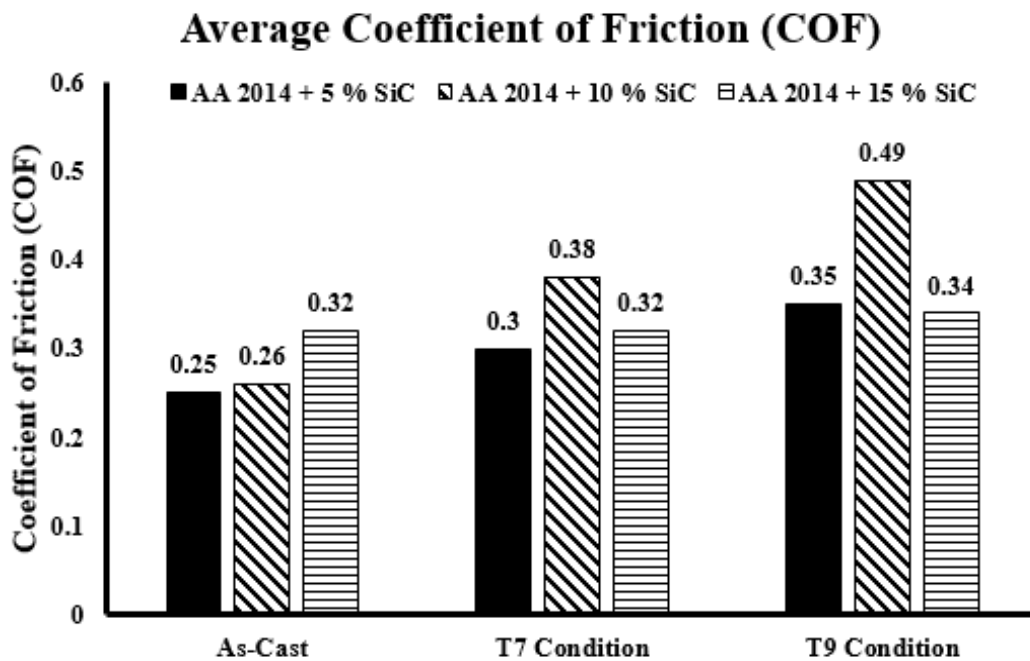

Figure 4.20 Plot of average coefficient of friction for as-cast, T7 processed and T9 processed composites

4.7 Summary

The manufactured as-cast composites were found to have several casting defects along with particle free regions and agglomeration of reinforcement particles. Thus, to enhance the metallurgical, mechanical and tribological properties of as-cast composites, FSP was performed. The study can be summarized as follows:

- Out of 10 trial experiments, two combinations of rotational speed and transverse speed i.e. 270 rpm and 78 mm/min (T7 condition) and 190 rpm and 50 mm/min (T9 condition) with the constant tool tilt angle of 2° gave promising results. Thus, it can be said that the range of process parameters to process as-cast composites is comparatively lower than that of aluminium alloys.

- Irrespective of the processing condition, the NZ of all processed composites revealed the presence of finer SiC particles having irregular shapes and sizes. NZ of T7 processed AA 2014 +5% SiC was found to have two different bands i.e. Band A and Band B. However, with the increase in weight percent of SiC particles, a reduction in the number of the band along with band thickness was observed in NZ of T7 processed composites. Compared to T7 processed, NZ of T9 processed AA 2014 + 5% SiC revealed a reduction in the number of alternating bands. With the increase in weight percent of reinforcement particles from 5% to 10%, the bands were disappeared and NZ was found to have particle rich and particle deficient zones. NZ of T9 processed AA 2014 + 15% SiC didn't revealed any bands or zones and SiC particles were homogeneously distributed in the entire NZ.

- When compared to as-cast composites, NZ of both processed composites revealed a significant reduction in grain size. As a result of stirring action generated by the rotating tool, the defects observed in as-cast composites were no more present in NZ of processed composites. The average grain size of as-cast composites were 61.95 μm, which was found to reduce in NZ of T7 processed AA 2014 + 5%, 10 and 15% SiC composites to 5.45 μm, 5.50 μm and 7.75 μm respectively. In the increasing order of weight percent of reinforcement particles, the observed grain size in NZ of T9 processed composites was 7.75 μm, 9.20 μm and 7.90 μm respectively.

- Compared to as-cast composites, only T7 processed AA 2014 + 10 % SiC and AA

2014 + 15% SiC composites revealed enhancement in microhardness. Irrespective of the weight percent of reinforcement particles, the microhardness of T9 processed composites were lower than that of T7 processed composites. Owing to higher grain size, a reduction in microhardness was observed for T9 processed composites. In the increasing order of reinforcement particles, the average microhardness of T7 processed composites was 81.25 Hv, 88.56 Hv and 86.97 Hv. Whereas, the microhardness of T9 processed composites was 75.36 Hv, 75.25 Hv and 81.98 Hv respectively.

- Except for T9 processed AA 2014 + 15% SiC, the rest of all processed composites revealed enhancement in wear resistance when compared to wear resistance of as-cast composites. It should also be noted that the wear resistance of T7 processed composites was much better than that of T9 processed composites. Owing to the homogenous distribution of reinforcement particles, finer grain size and minimum processing defects, higher wear resistance was observed for T7 processed composites. Irrespective of the processing condition, the wear resistance was found to increase with the increase in weight percent of reinforcement particles from 5% to 10%. However, a further increase in weight percent from 10% to 15% was found to have an adverse effect on wear resistance. The average wear of T7 processed composites in the increasing order of weight percent of reinforcement particles was 376 microns, 230 microns and 247 microns respectively. In the same line, the wear of T9 processed composites was 405 microns, 227 microns and 402 microns respectively.

- It was observed that post FSP, either the COF was found to increase or was unaffected. Similar to wear, COF also followed a similar trend. Irrespective of the processing condition, with the increase in weight percent of reinforcement particles from 5% to 10%, the COF was found to increase. However, further increase in weight percent from 10% to 15%, reduction in COF was observed.